Stress and Deformation Behavior of 2D Composite Cellular Actuator Structures of Ceramic Building Blocks and Epoxy Resins

Franziska Eichhorn, Helmut Schiegerl, David Köllner, Ken-ichi Kakimoto, and Tobias Fey*

2D actuator composite structures are fabricated of lead zirconate titanate (PZT) and Al_2O_3 building blocks with an epoxy resin matrix. This novel modular concept gives the possibility to create complex geometric structures where the structure itself tailors the physical properties. To improve the possibilities of excitation or loading and determine the influence of the geometric parameters as slenderness ratio $t_2 \cdot g^{-1}$ and active area A_{active} finite element (FE) simulations are used. The stress distribution σ_{yy} within the unit cell and the resulting strain amplification a_y are tested with different mechanically coupled thermal excitation modes. A homogeneous excitation of the PZT building blocks and a maximum A_{active} of 24% led to a maximum of strain amplification and a reduction of induced tensile stresses. In addition, zero deformation could be generated by modifying the structure design with a slenderness ratio of 0.5. Further geometric variations offer the potential to increase the strain amplification.

1. Introduction

The physical properties of 2D cellular solids with ordered cell designs are determined by the selected materials and their architecture.[1,2] Outstanding mechanical properties make them suitable for different applications with low weight, damage tolerance, and impact resistance.[1,3–8] In particular their mechanical deformation behavior[3,4] can be used to increase elongation or

F. Eichhorn, H. Schiegerl, D. Köllner, T. Fey
Department of Material Science and Engineering
Institute of Glass and Ceramics
Friedrich-Alexander-Universität Erlangen-Nürnberg
Martensstr. 5, D-91058 Erlangen, Germany
E-mail: tobias.fey@ww.uni-erlangen.de

K. Kakimoto, T. Fey
Frontier Research Institute for Materials Science
Nagoya Institute of Technology
Gokiso-cho, Showa-ku, Nagoya 466-8555, Japan

The ORCID identification number(s) for the author(s) of this article can be found under https://doi.org/10.1002/pssb.202100591.

contraction compared with dense materials.[7,9–11] Optimization of geometry parameters and material variations are performed using FE simulations to analyze deformation behavior and stress distribution.[12–19] Idealized and periodically arranged cellular solids were analyzed using different analytical and experimental models.[1,2,12–15,20–25]

A novel field of research addresses the modular assembly of cellular ceramic structures from individual macroscopic building blocks into which the corresponding structure is disassembled. These modular units named as building blocks can be individually functionalized and excited.[24,25] Eichhorn et al.[24,25] investigated such novel structures through finite element (FE) simulations and determined the strain amplification and stress behavior as a function of geometric parameters such as the slenderness ratio $t_2 \cdot g^{-1}$. These periodic cellular structures were parameterized and with the support of algorithms different variants of the geometric structure could be generated.[24,25]

Gohari et al.,[26] Ray et al.,[27] and Steiger et al.[28] used numerical models and FE simulations as ABAQUS to investigate plate- and bar-shaped, dense composite actuator models made consisting of lead zirconate titanate (PZT) fibers in an epoxy resin matrix. FE simulations were compared with various mathematical theories to verify the models.

In this work, PZT epoxy resin actuator models[26,27] were combined with cellular structures[24,29] and modular structures built up with building blocks[24,30] to fabricate cellular composites. Nonlinear FE simulations were used to investigate their strain amplification and stress behavior. Numerical FEA is used here as a tool. Therefore, the focus is on the generation of these novel structures.

These 2D modular and cellular actuator structures with a relative density of 0.445 were assembled of individual ceramic building blocks connected with epoxy resin. The optimization of the structure was performed by parameter variation to generate maximum strain gain under mechanically coupled thermal excitation. Following Eichhorn et al.,[24,25] it was assumed for the simulations that the thermal expansion correlates directly with the piezoelectric expansion due to the crystalline material structure. The variations in strain amplification as well as stress

distribution were determined in the middle unit cells to minimize the edge influence.

2. Experimental Section

Ceramic building blocks were produced using PZT and Al_2O_3 injection mold according to our invented methods,[24,25,31,32] as shown in **Figure 1**.

According to the dimensions of the modular building blocks, the structure of the planar actuator was divided so that it can be assembled from different building blocks. These were parallel, horizontally oriented alumina crossbars (frame: L_{ges}, t_1) and three piezoceramic PZT beams (column, lever: h, t_1, t_2) and they were bonded by epoxy resin with a thickness $v = 0.10$ mm, as shown in Figure 1 and **Table 1**. The cellular structures were 2D, whereas the building blocks had a thickness b of 5.00 mm.

The material properties of PZT, Al_2O_3, and epoxy resin are reported in the study by Eichhorn et al.[24] Here, the actuator model and the algorithms (using scripting language "Python" [Version 3.5, Python Software Foundation, Beaverton, Oregon, USA]) to generate the simulation models are described, too. The model generation was controlled by so-called procedure files, where besides the structure generation, the material properties, boundary conditions, as well as the meshing parameters were assigned.

The optimization of the design was carried out under variation of the geometric slenderness $t_2 \cdot g^{-1}$ and three modes of mechanically coupled thermal excitation which was simulated with the commercial software "MarcMentat" (Version 2017.0.0, MSC Software, Munich, Germany), which was used for over 25 years in industry and science,[33–35] as shown in Table 1. For meshing of this nonlinear plane strain calculation, the triangle element type six of the element class three (second-order isoparametric 2D plane strain triangular element) according to "MSC Element Library" was used. The 2D elements were arranged by the internal mixed-mesh-maximum principal by validated mesh optimization based on the defined subdivisions in the geometry model.
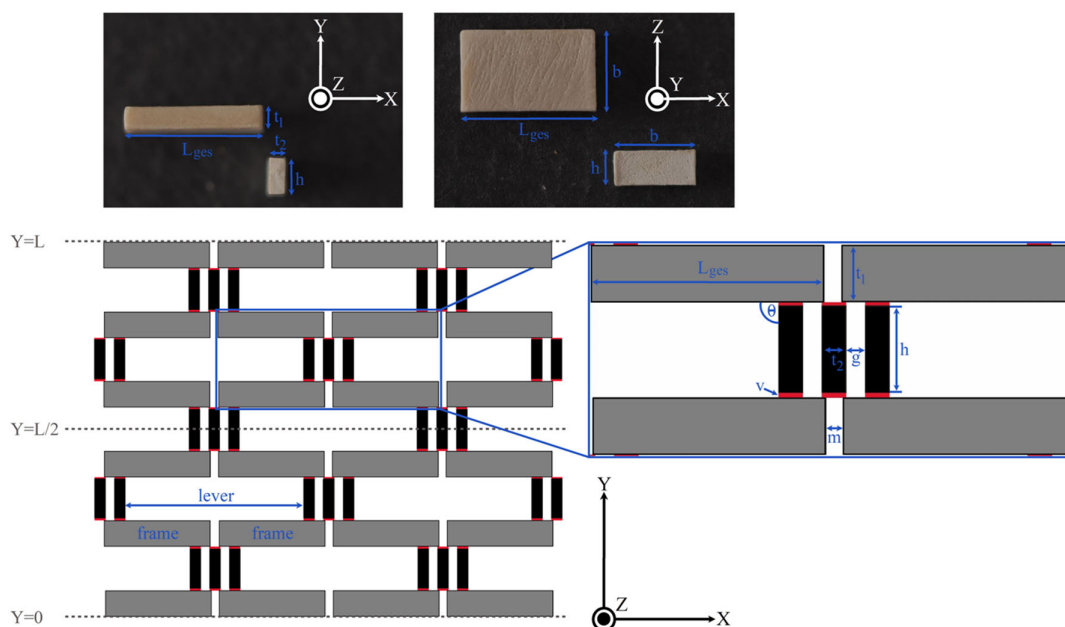
Table 1. Geometric parameters of the 2D cellular actuator structure.

Geometric parameter	Value	Unit
g	0.10–6.92	mm
t_1, t_2	1.50	mm
$t_2 \cdot g^{-1}$	0.22–15.00	–
$\rho_{relative}$	0.445	–
L_{ges}	10.00	mm
h	2.50	mm
m	0.30	mm
v	0.10	mm
Θ	0	°

Table 2. Simulated thermal excitation and corresponding active areas A_{active} depending on excitation mode.

Excitation mode	E | E | N	E | S | N	E | N | N
Lever	$\alpha = +$, E	$\alpha = +$, E	$\alpha = +$, E
Strut	$\alpha = +$, E	$\alpha = -$, S	$\alpha = 0$, N
Frame	$\alpha = 0$, N	$\alpha = 0$, N	$\alpha = 0$, N
Active area A_{active}	0.24	0.24	0.16

Figure 1. Used modular actuator model built with two types of building blocks: Al_2O_3- (grey) and PZT-building blocks (black). The epoxy phase is colored in red.

The simulation conditions were as follows: 1) The calculation was carried out in plane strain mode. 2) The nodal movement was set to zero for all nodes with y-coordinate $Y = 0$ and $Y = L$, Figure 1. 3) Thermal expansion of frame $\alpha_{thermal}$ was set to $0\,K^{-1}$ (Neutral). Therefore, no excitation was applied, and the frame remained in its original state. There was neither expansion nor shrinkage. The frame deformed solely through the deformation of the columns and levers. 4) Columns and levers

were exposed to a temperature change with a constant temperature gradient ΔT of 15 K. 5) For expansion mode, $\alpha_{thermal}$ was set as $+76 \times 10^{-6}\,K^{-1}$ and for Shrinkage mode, $\alpha_{thermal}$ as $-76 \times 10^{-6}\,K^{-1}$. 6) This resulted in the three different excitation modes (E|E|N), (E|S|N), and (E|N|N), as shown in Table 1.

Due to the individual excitation of the modular units, the proportion of the active area A_{active} was reduced (expansion, shrinkage) and only a part of the structure was active, where
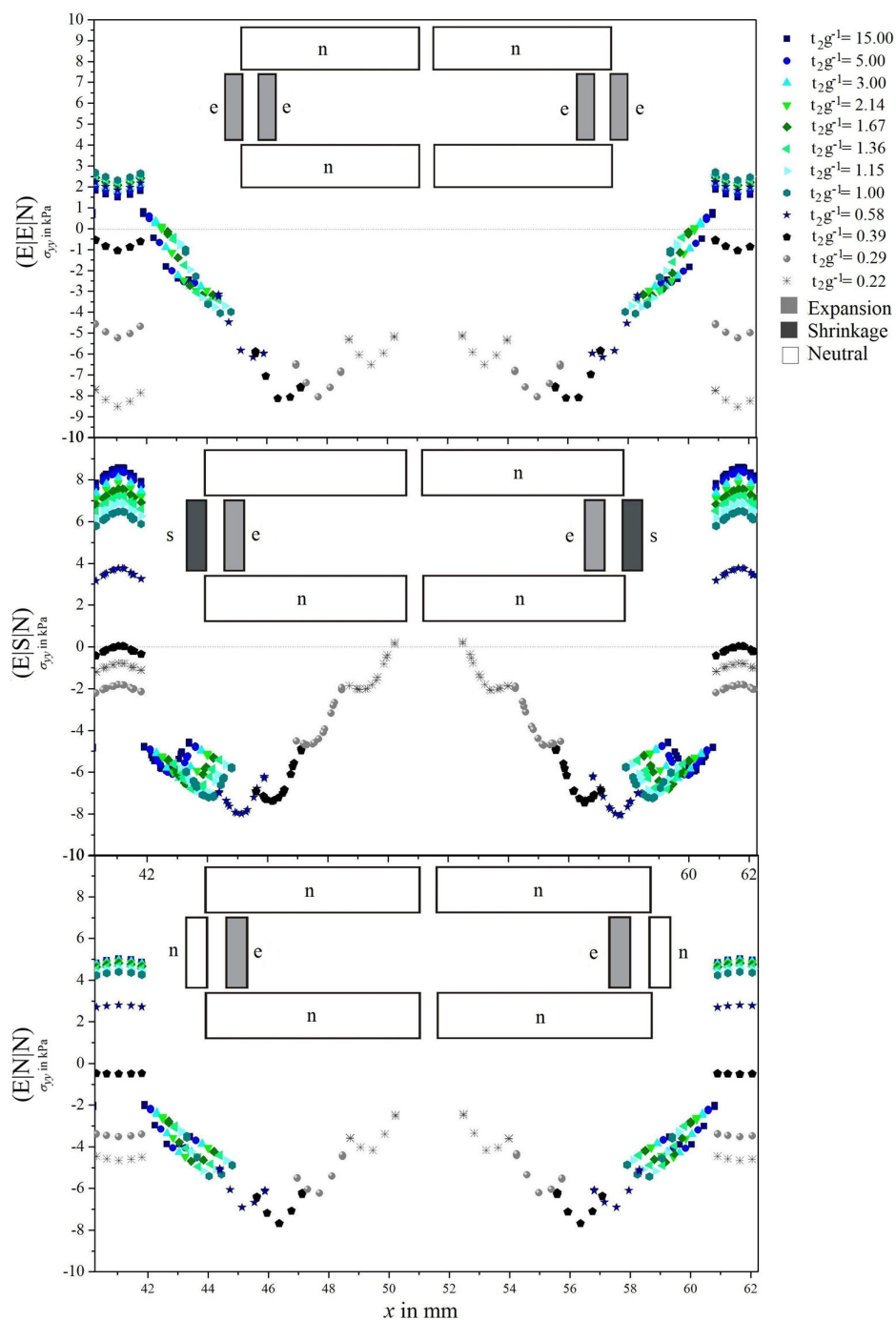

Figure 2. Stress distribution in σ_{yy} under mechanically coupled thermal excitation modes (E|E|N), (E|S|N) and (E|N|N) of Al_2O_3–PZT composite actuator structures and in dependence of $t_2 \cdot g^{-1}$.

$A_{\text{active}} < A_{\text{lattice}}$. The analyzed modes (E|E|N) and (E|S|N) had an A_{active} of 24% and (E|N|N) of 16% compared with the whole structure area.

The parameter of slenderness ratio $t_2 \cdot g^{-1}$ varied between 0.22 and 15.00. Therefore, the thicknesses t_1 and t_2, the angle θ, and the other geometric parameters v, gap m, L_{ges}, and h were kept constant to limit the variations of the actuator model, as shown in Table 1. The mode (E|S|N) activated levers and columns contrarious, as shown in **Table 2**. The (E|E|N) and (E|S|N) mode had a constant active component and different excitations of the columns.

3. Results and Discussion

3.1. Stress Distribution under Different Excitation Modes

The excitation mode and the slenderness ratio $t_2 \cdot g^{-1}$ influenced the calculated stress distributions σ_{yy} through the cross section of the middle, as shown in **Figure 2**. The deformation in the Al$_2$O$_3$–PZT structures showed a stress distribution of σ_{yy} in the range from $-8.27\,\text{kPa}$ ($t_2 \cdot g^{-1} = 0.22$) to $+2.69\,\text{kPa}$ ($t_2 \cdot g^{-1} = 1.00$) for (E|E|N) mode, for (E|S|N) mode in the range from $-8.23\,\text{kPa}$ ($t_2 \cdot g^{-1} = 0.58$) to $+9.04\,\text{kPa}$ ($t_2 \cdot g^{-1} = 15.00$), and in the range from $-7.68\,\text{kPa}$ ($t_2 \cdot g^{-1} = 0.39$) to $+5.03\,\text{kPa}$ ($t_2 \cdot g^{-1} = 5.00$) for (E|N|N) mode.

It can be determined from the simulation results that an inflection point with minimum stresses occur inside the levers for (E|E|N) and (E|N|N) modes at $t_2 \cdot g^{-1} = 0.39$ (ratio of a "golden ratio") and for (E|S|N) mode at $t_2 \cdot g^{-1} = 0.58$. With a reduction of A_{active} of 8%, absolute internal compressive stresses decreased by about 10%, whereas the tensile stresses inside the levers increased up to 46% when changing from (E|E|N) to (E|N|N) mode. In the (E|S|N) mode, tensile stresses occurred for $t_2 \cdot g^{-1} < 0.58$ and compressive stresses for $t_2 \cdot g^{-1} > 0.58$ in the range from $+8.66$ to $-2.22\,\text{kPa}$. Decreasing $t_2 \cdot g^{-1}$, the absolute values of the compressive stresses within the levers increased to a maximum of $-8.15\,\text{kPa}$.

The opposite excitation in (E|S|N) mode increased the tensile stresses by 322% and reduced the compressive stresses by 73% compared with the (E|N|N) mode with a shifting of the inflection point for slenderness $t_2 \cdot g^{-1}$ change of 38%. In contrast to the lattice structures, the resulting σ_{yy} was about 99% significantly lower for the same applied ΔT.

3.2. Strain Amplification Behavior

Strain amplification a_y is defined as the strain increase in the cellular structure as opposed to a dense monolithic material. Following Eichhorn et al.,[24] this is calculated as the quotient of the strain of the lattice $\varepsilon_y^{\text{lattice}}$ and the strain of the dense material $\varepsilon_y^{\text{dense}}$ as well as the active area and relative density. Due to the sole lateral dynamic excitation, the deformation in X-direction is nearly zero for all three excitation modes. The normal strains were also close to zero due to pure flexural deformation. Hence, the deformation behavior in the X-direction was neglected.

The strain amplification a_y decreased for all three modes with increasing $t_2 \cdot g^{-1}$, as shown in **Figure 3**. The (E|E|N) and (E|N|N)
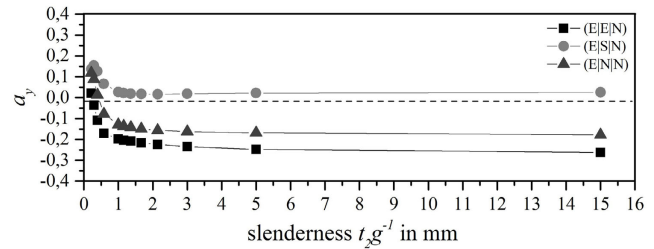

Figure 3. Strain amplification a_y of Y-direction in dependence of the gap width $t_2 \cdot g^{-1}$.

mode caused negative strain amplifications for high $t_2 \cdot g^{-1}$. Applying the (E|E|N) mode inside the slenderness range 0.22–15.00, a_y was reduced from $+0.021$ down to -0.263 with zero elongation at $t_2 \cdot g^{-1} = 0.57$. The (E|N|N) mode showed a similar trend within a range of 0.119 down to -0.178. The reduced active area here caused a reduction of $|a_y|$ of 32%.

Due to the contrarious deformation of the columns and levers in (E|S|N) mode, the strain amplification increases from $+0.017$ to $+0.154$ with increasing $t_2 \cdot g^{-1}$.

For all three modes, a saturation of a_y was reached for high slenderness ratios due to the small distances between columns and levers. By increasing the distance g and decreasing $t_2 \cdot g^{-1}$ between the column and lever, the influence of the individual components increased.

4. Conclusion

In this article, modular actuator structures were fabricated from PZT and Al$_2$O$_3$ building blocks connected by a thin epoxy layer and their properties calculated by FE simulations. The influence of the excitation mode, slenderness, and active area on strain amplification and stress distribution was investigated by mechanically coupled thermal excitation.

The highest negative strain amplification of $a_y = -0.263$ was determined in (E|E|N) mode and the highest positive strain amplification in (E|S|N) of $a_y = +0.154$ for $t_2 \cdot g^{-1} = 15.00$. A decrease in $t_2 \cdot g^{-1}$ and minimizing the active area decreased the induced internal tensile stresses. For all excitation modes, a point of inflection of the stresses occurred at the ratio of the "golden ratio" ($t_2 \cdot g^{-1} = 0.39$). By minimizing the active part of 8%, $|a_y|$ was decreased by 32%. Only the modes (E|E|N) and (E|N|N) showed zero strain amplification for different slenderness ratios, which allows the generation of strain-resistant complex structures.

Conflict of Interest

The authors declare no conflict of interest.

Data Availability Statement

The data that support the findings of this study are available from the corresponding author upon reasonable request.

[1] T. A. Schaedler, W. B. Carter, *Annu. Rev. Mater. Res.* **2016**, *46*, 187.
[2] A. E. Simone, L. J. Gibson, *Acta Mater.* **1998**, *46*, 2139.
[3] L. J. Gibson, M. F. Ashby, G. S. Schajer, C. I. Robertson, *Proc. R. Soc. A* **1982**, *382*, 25.
[4] L. J. Gibson, M. F. Ashby, *Cellular Solids: Structure and Properties*, Cambridge University Press, Cambridge **1999**, Chapter 4, pp. 93–174.
[5] W. Yang, Z.-M. Li, W. Shi, B.-H. Xie, Yang Ming-Bo, *J. Mater. Sci.* **2004**, *39*, 3269.
[6] B. Pan, K. Qian, H. Xie, A. Asundi, *Meas. Sci. Technol.* **2009**, *20*, 62001.
[7] B. Haghpanah, J. Papadopoulos, D. Mousanezhad, H. Nayeb-Hashemi, A. Vaziri, *Proc. R. Soc. A* **2014**, *470*, 20130856.
[8] J. Penzien, T. Didriksson, *AIAA J.* **1964**, *2*, 531.
[9] V. S. Deshpande, M. F. Ashby, N. A. Fleck, *Acta Mater.* **2001**, *49*, 1035.
[10] A. G. Evans, J. W. Hutchinson, M. F. Ashby, *Prog. Mater. Sci.* **1999**, *43*, 171.
[11] H. Wadley, N. A. Fleck, A. G. Evans, *Compos. Sci. Technol.* **2003**, *63*, 2331.
[12] O. C. Zienkiewicz, R. L. Taylor, *The Finite Element Method for Solid and Structural Mechanics*, 6th ed., Elsevier Butterworth-Heinemann, Amsterdam **2005**.
[13] A. Ajdari, P. Canavan, H. Nayeb-Hashemi, G. Warner, *Mater. Sci. Eng., A* **2009**, *499*, 434.
[14] A. E. Simone, L. J. Gibson, *Acta Mater.* **1998**, *46*, 3929.
[15] M. J. Silva, L. J. Gibson, *Int. J. Mech. Sci.* **1997**, *39*, 549.
[16] M. Grediac, *Int. J. Solids Struct.* **1993**, *30*, 1777.
[17] D. Ruan, G. Lu, B. Wang, T. X. Yu, *J. Impact Eng.* **2003**, *28*, 161.
[18] K. Li, X.-L. Gao, G. Subhash, *Int. J. Solids Struct.* **2005**, *42*, 1777.
[19] B. M. Goldsberry, M. R. Haberman, *Int. J. Appl. Phys.* **2018**, *123*, 091711.
[20] N. A. Nascimento, J. Belinha, R. M. Natal Jorge, D. E. S. Rodrigues, *Eng. Anal. Bound. Elem.* **2021**, *129*, 27.
[21] H. Salem, D. Boutchicha, A. Boudjemai, *Int. J. Interact. Des. Manuf.* **2018**, *12*, 955.
[22] C. Baumgart, T. Halle, C. Weigelt, L. Krüger, C. G. Aneziris, *Cell. Mater.* **2018**, *30*, 35.
[23] J. J. Andrew, H. Alhashmi, A. Schiffner, S. Kumar, V. S. Deshpande, *Mater. Des.* **2021**, *208*, 109863.
[24] F. Eichhorn, F. Keppner, D. Köllner, T. Fey, *Adv. Eng. Mater.* **2021**, *24*, 2100536.
[25] F. Eichhorn, F. Keppner, *Adv. Eng. Mater.* **2022**, *24*, 2270004.
[26] S. Gohari, S. Sharifi, R. Abadi, M. Izadifar, C. Burvill, Z. Vrceli, *Smart Mater. Struct* **2018**, *27*, 095004.
[27] M. C. Ray, N. Mallik, *AIAA J.* **2004**, *42*, 1398.
[28] K. Steiger, P. Mokrý, in *2011 10th International Workshop on Electronics, Control, Measurement and Signals (ECMS)*, CD Proceedings, IEEE, Piscataway, NJ **2011**, https://doi.org/10.1109/IWECMS.2011.5952380.
[29] T. Fey, F. Eichhorn, G. Han, K. Ebert, M. Wegener, A. Roosen, K. Kakimoto, P. Greil, *Smart Mater. Struct.* **2008**, *25*, 015017.
[30] M. Götz, Dissertation, Friedrich-Alexander Universität Erlangen-Nürnberg, **2014**.
[31] M. Stumpf, X. Fan, J. Biggemann, P. Greil, T. Fey, *J. Eur. Ceram. Soc.* **2019**, *39*, 2003.
[32] J. Biggemann, B. Diepold, M. Pezoldt, M. Stumpf, P. Greil, T. Fey, *J. Am. Ceram. Soc.* **2018**, *101*, 3864.
[33] J. Biggemann, D. Köllner, J. Schatz, M. Stumpf, T. Fey, *Mater. Lett.* **2021**, *303*, 130529.
[34] J. Biggemann, M. Stumpf, T. Fey, *Materials* **2021**, *14*, 3294.
[35] T. Fey, M. Stumpf, A. Chmielarz, P. Colombo, P. Greil, M. Potoczek, *J. Eur. Ceram. Soc.* **2018**, *38*, 3424.